Experimental Studies on Wake-Induced Bypass Transition of Flat-Plate Boundary Layers under Favorable and Adverse Pressure Gradients*

Eitaro KOYABU**, Ken-ichi FUNAZAKI*** and Manabu KIMURA****

This study investigates wake-induced bypass transition of boundary layers on a flat plate which is subjected to favorable and adverse pressure gradients. Inlet free-stream turbulence level is controlled with a turbulence grid. Detailed boundary layer measurements are executed by use of a single hot-wire probe. The main focus of this paper is on how and to what extent the wake-induced bypass transition of a flatplate boundary layer can be affected by favorable - adverse pressure gradient as well as enhanced turbulence intensity. A spoked-wheel-type wake generator creates periodic wakes in front of the flat plate. Two types of the wakes are generated by altering the direction of the movement of the wake-generating bars. Instantaneous velocity signals successfully reveal the flow events associated with the wake passage happening inside the boundary layer, such as the emergence of turbulent spots and calmed regions behind them. Noticeable differences in the transitional behavior due to the wake passage also appear between these two types of the wakes.

Key Words: Boundary Layer, Wake, Bypass Transition, Pressure Gradient, Measurement

1. Introduction

According to Mayle's categorization[1], there are several paths of boundary layer transition to turbulence observed in turbomachines, and so-called bypass transition is one of the transition paths there. In bypass transition, turbulent spots are believed to be created in the boundary layer as a direct consequence of, for example, elevated free-stream turbulence level. In other words, the stage of conventional two-dimensional Tollmien-Schlichting instability is bypassed in this type of transition process. Since flow fields in turbomachines are characterized with the existence of intense external disturbances such as free-stream turbulence and periodic wakes, it is easy to realize that bypass transition mode dominates the transition process of blade boundary layers. Therefore, a number of studies have been made on wake-induced bypass transition of blade boundary layer[1]-[6]. Recently, Ottavy et al.[7] executed experimental and numerical work upon moving-bar wake interaction with a boundary layer on a flat plate subjected to a pressure gradient emulating a compressor blade. Their efforts, however, did not elucidate the effects of the pressure gradient upon the development of wake-induced boundary layer transition under the influence of free-stream turbulence.

In the present study, the experimental study was performed on the wake-induced bypass transition of the boundary layer on a flat-plate test model subjected to periodic wake passing. The unsteady velocity field was measured with hot-wire anemometry. A passage-contouring device similar to that used in Ottavy et al.[7] was adopted to generate a pressure gradient on the test model which was typical to an aft- or front-loaded turbine blade. A spoked-wheel type wake generator, consisting of a disk and several cylindrical bars, produced two types of the incoming wakes against the test model by altering the direction of the disk rotation. A turbulence grid was introduced in a case to enhance free-stream turbulence.

2. Nomenclature

d : diameter of the wake-generating bar
$C_p(x)$: pressure coefficient
C_v : coefficient

* Received 2nd February, 2004 (No. 04-4049)
** Department of Mechanical Engineering, Sophia University, 7-1 Kioicho, Chiyoda-ku 102-8554, Japan
*** Department of Mechanical Engineering, Iwate University, 3-5 Ueda 4, Morioka 020-8551, Japan
**** Sony Shiroishi Semiconductor Co., 53-2 Shiratori 3, Shiroishi 989-0734, Japan

$D(t)$: detector function
f : wake-passing frequency ($=nn_b/60$)
$K(x)$: acceleration parameter
L : length of the test model (= 1 m)
N : number of sampled data
n : rotation per minute
n_b : number of wake-generating bars
p_0, $p(x)$: stagnation pressure, static pressure on the test plate
Re_{in} : Reynolds number based on the length of the test model and the inlet velocity
Re_2 : Reynolds number based on the steady-state momentum thickness and the local velocity
St : Strouhal number ($=fL/U_{in}$)
t : time
T : wake-passing period ($=1/f$)
T_v : threshold
$\widetilde{Tu}$: ensemble-averaged turbulence intensity
U_{in} : inlet velocity
$U_e(x)$: local velocity
u_k : sampled velocity data
$\tilde{u}$: ensemble-averaged velocity
X : longitudinal distance from the leading edge
x : surface length from the leading edge
y : distance from the surface of the test model
$\tilde{\delta}$: ensemble-averaged boundary layer thickness
ν : kinetic viscosity

Subscripts

$\bar{f}$: time-averaged value
$\tilde{f}$: ensemble-averaged value

3. Experimental Setup

Figure 1 shows a schematic layout of the test apparatus used in this study. The settling chamber and the contraction nozzle reduced free-stream turbulence down to about 0.5%. Free-stream turbulence intensity was controlled using a passive-type turbulence grid. Periodic wakes were produced by a spokenwheel type generator that consisted of a disk with 400 mm diameter and cylindrical bars of 5 mm or 3 mm diameter. Revolution number of the disk in the wake generator was counted by an optical tachometer. The fluctuation in revolution was found to be less than 0.5%. Figure 2 shows the test model, the wake generator and passage-contouring devices attached on the top and bottom walls of the test duct. The wake generator was set so that each of the wake generating bars became parallel with the leading edge of the test model when it moved in front of the model. Rotation direction of

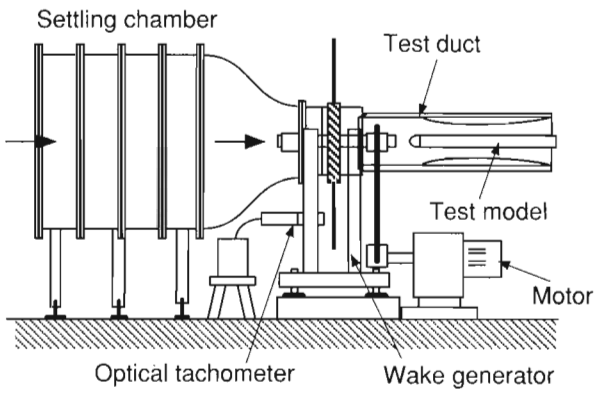

Fig. 1 Test facility

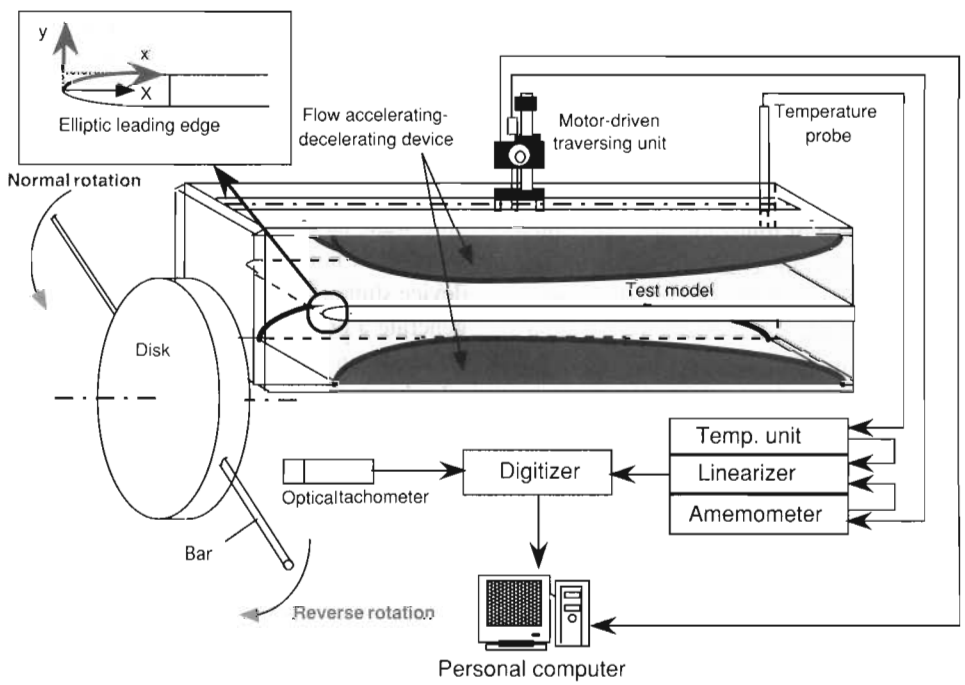

Fig. 2 Test apparatus and measurement system

the disk of the wake generator was easily reversed, which changed the movement of the wake-generating bars relative to the model, as designated *normal rotation* or *reverse rotation* in Fig. 2. The test model, made of acrylic-resin plates, was 1.0 m long. It had a semi-elliptic leading edge with the long axis of 75 mm and the short axis of 15 mm, followed by a flat-plate after body. The width and thickness were 200 mm and 30 mm, respectively. Static pressure taps were provided on one side of the test model to measure the pressure distribution on the test surface. The passage-contouring devices were shaved out of styrofoam bricks so as to take a shape for establishing a pressure gradient typical to an aft-loaded turbine blade, at first. It did not take long time, however, to realize that another type of pressure gradient could be achieved only by turning it around, the pressure gradient which seemed to correspond to that on a front-loaded turbine blade. Also shown in Fig. 2 is the system for the boundary layer measurement based on hot-wire anemometry. The passagecontouring device had a slot along its centerline through which a hot-wire probe could be inserted into the main flow.

4. Instrumentation and Data Processing

4.1 Ensemble-averaged quantities

A single hot-wire probe was used to measure the boundary layer on the test model. PC-controlled traversing unit placed the probe to the location to be measured with the precision of 0.01 mm. The probe was connected to a constant-temperature anemometer. By monitoring the free-stream temperature at the exit of the test section, the temperature unit effectively compensated temperature fluctuation of relatively low frequency during the long-running measurement. The A/D converter acquired and digitized linearized signal from the probe using once-per-revolution signal from the optical tachometer as synchronization signal, which guaranteed the application of the phase-locked averaging technique to the sampled data. The data-sampling rate was 50 kHz and each of the digitized records contained 2 500 words. Phase-locked or ensemble-averaged velocity, $\tilde{u}$, was then calculated from the acquired instantaneous velocity data, u_k ($k = 1,2,\ldots,N$), as follows:

$$\tilde{u}(x,y,t) = \frac{1}{N}\sum_{k=1}^{N} u_k(x,y,t), \quad N = 100 \tag{1}$$

Ensemble-averaged turbulence intensity was also defined by

$$\widetilde{Tu}(x,y,t) = \frac{1}{U_e(x)}\sqrt{\frac{1}{N-1}\sum_{k=1}^{N}\{u_k(x,y,t)-\tilde{u}(x,y,t)\}^2}, \tag{2}$$

where $U_e(x)$ was the local velocity determined from the static pressure measurements with the Bernoulli's equation. From the ensemble-averaged velocity, ensemble-averaged boundary layer thickness $\tilde{\delta}(x,t)$ was determined, which was defined as the distance from the test model surface to the location where the ensemble-averaged velocity reached the maximum among the data acquired at the same streamwise location.

4.2 Time-averaged quantities

Time-averaged quantities were obtained by the integration of the ensemble-averaged quantities over the wake-passing period. For instance, time-averaged boundary layer thicknesses were calculated by

$$\bar{\delta}(x) = \frac{1}{T}\int_0^T \tilde{\delta}(x,t)dt \tag{3}$$

4.3 Intermittency factor

The raw velocity data contained useful information to understand transitional process of the wake-affected boundary layer in detail. In order to quantify this transitional process, an intermittency factor was introduced, which could be regarded as the ratio of total sum of the time when the boundary layer was turbulent to the whole measurement time period. Calculation of the intermittency factor required a detector function as well as a proper threshold to judge whether the boundary layer concerned was laminar or turbulent. Eventually, the following procedure was adopted to determine the local intermittency factor $\gamma(x,t)$.

$$\gamma(x,t) = \frac{1}{N}\sum_{k=1}^{N} I_k(x,t) \tag{4}$$

$$I_k(x,t) = \begin{cases} 1 & \text{when } D(t) \geq T_v \\ 0 & \text{when } D(t) < T_v \end{cases}, \tag{5}$$

where turbulence detector function $D(t)$ and threshold level T_v were defined in consideration of the previous works (for example, Solomon[3]) by the following equations, respectively.

$$D(t) = \left|\frac{\partial u_k}{\partial t}\right|_{smooth}, \tag{6}$$

$$T_v = C_v(U_e^2/\bar{\delta}) \quad C_v = 0.10, \tag{7}$$

where $|\partial u_k/\partial t|_{smooth}$ was calculated by averaging the value of $|\partial u_k/\partial t|$ over a series of short window times. These window times t_w were determined using a time scale associated with the largest eddies in the boundary layer, which was

$$t_w = 2.5(\bar{\delta}/U_e). \tag{8}$$

The basic concept of the technique introduced in the above was first developed by Falco and Gendrich[15], then modified by Solomon[3] so as to deal with cases of wake-induced boundary layer transition. The ability of this technique is widely accepted, in particular among the turbomachinery research community[16], however, some arbitrariness surely exists in terms of the selection of the value of C_v. In fact, several attempts eventually led to the value of 0.10 for C_v adoped in this study, which was smaller than the recommended value by Solomon ($C_v = 0.15$). Figure 3

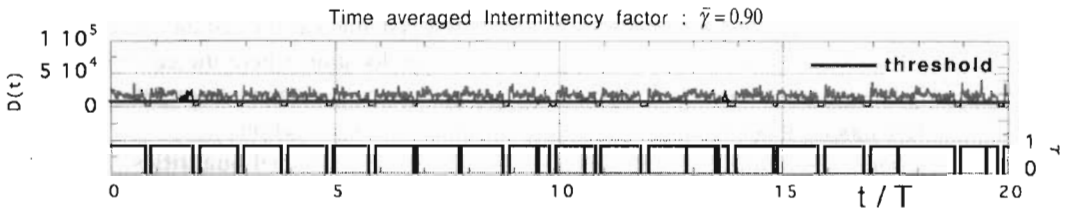

Fig. 3 An example for detecting turbulent zones in the instantaneous velocity data

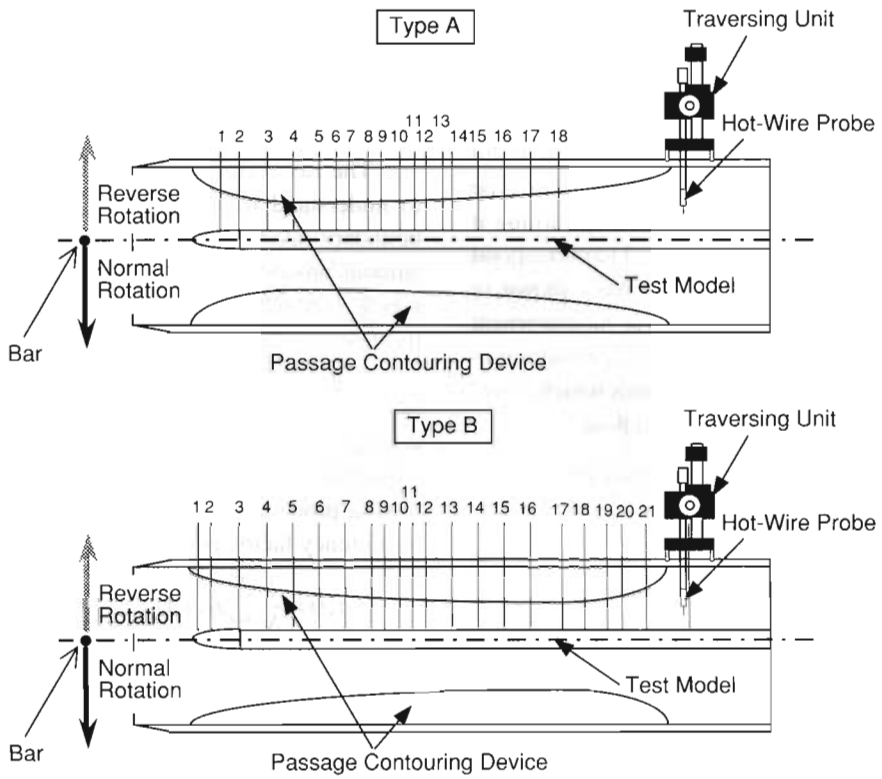

Fig. 4 Passage-contouring device and measurement locations

is an example of $D(t)$ and a series of steps showing turbulent zones that possessed high velocity acceleration with more than the threshold given by Eq. (7).

The onset and the end of transition were then determined in this study as the locations where time-averaged intermittency factor $\overline{\gamma(x)}$ exceeded 0.025 and 0.975, respectively. These two values were selected in an empirical manner using instantaneous velocity data so that they could reasonably detect the transition.

4.4 Uncertainty

Uncertainties of the inlet velocity and instantaneous velocity were estimated to be about 2% and 3% using the Kline and McClintock method[8].

4.5 Test Conditions

Table 1 shows the test conditions of this study. Test Case 1 was the baseline experiment with no wake, where the inlet velocity U_{in} was 10 m/s and Reynolds number Re based on the length of the test model and the inlet velocity was 6.7×10^5. The passage contouring device, which was referred to as Type A in this case and is shown in the upper of Fig. 4, was set so as to achieve a front-loading type pressure gradient on the test model. Effects of incoming wakes for the normal rotation mode were investigated in Test Case 2. Strouhal number, which characterized wake-affected unsteady flow field over the test mode and was defined by

$$St=\frac{fL}{U_{in}}=\frac{nn_b}{60}\frac{L}{U_{in}}, \tag{9}$$

was 2.0, where the disk rotational speed n was 600 rpm and the bar count n_b was 2. Since the horizontal distance between the center of the disk of the wake gen-

Table 1 Test conditions

Test Case	Rotation Direction	St	Tu	Passage Contouring	d
1	-	0.0	0.5%	Type-A	
2	Normal	2.0	0.5%	Type-A	5 mm
3	-	0.0	0.5%	Type-B	
4	Normal	2.0	0.5%	Type-B	3 mm 5 mm
5	Reverse	2.0	0.5%	Type-B	
6	-	0.0	1.4%	Type-B	
7	Normal	2.0	1.4%	Type-B	3 mm 5 mm

Table 2 Measurement locations for Type A and Type B

Type A		Type B	
station	x / L	station	x / L
1	0.065	1	0.020
2	0.105	2	0.050
3	0.155	3	0.100
4	0.205	4	0.150
5	0.255	5	0.200
6	0.285	6	0.250
7	0.315	7	0.300
8	0.345	8	0.350
9	0.375	9	0.375
10	0.405	10	0.400
11	0.435	11	0.425
12	0.46	12	0.450
13	0.485	13	0.500
14	0.505	14	0.550
15	0.555	15	0.600
16	0.605	16	0.650
17	0.705	17	0.710
18	0.755	18	0.750
		19	0.790
		20	0.830
		21	0.870

erator and the duct centerline was 363 mm, the moving speed of the bar on the centerline was 22.8 m/s. Test case 3 was different from Test case 1 only with respect to the arrangement of the passage-contouring device, which created aft-loading type pressure gradient and was called Type-B. Test Cases 4 and 5 aimed at clarification of the effects of the bar movement upon the boundary layer transitional behavior under relatively low free-stream turbulence. The inlet free-stream turbulence intensity was increased by 28% in Test Cases 6 and 7, each of which corresponded to Test Cases 3 and 4, respectively.

The measurement region extended from $x/L=0.105$ to $x/L=0.875$ in the streamwise direction and from $y/L=0.2\times10^{-3}$ to $y/L=10\times10^{-3}$ in the vertical direction. Table 2 provides detailed information on the streamwise locations of the boundary layer measurements for Type A as well as Type B.

Figure 5 shows distributions of measured pressure coefficient $C_p(x)$ as well as the resultant acceleration parameter $K(x)$ over the test model, where $C_p(x)$ and $K(x)$ were calculated by

$$C_p(x)=\frac{p_0-p(x)}{1/2\rho U_{in}^2}=\left(\frac{U_e(x)}{U_{in}}\right)^2, \tag{10}$$

$$K(x)=\frac{\nu}{U_e(x)^2}\frac{dU_e(x)}{dx}, \tag{11}$$

respectively. The flow field induced by Type A was characterized by the existence of abrupt flow acceleration exceeding 3×10^{-6} just after the leading edge of the test model, followed by gradual flow deceleration. The averaged acceleration parameter of Type A was about 5×10^{-7}.

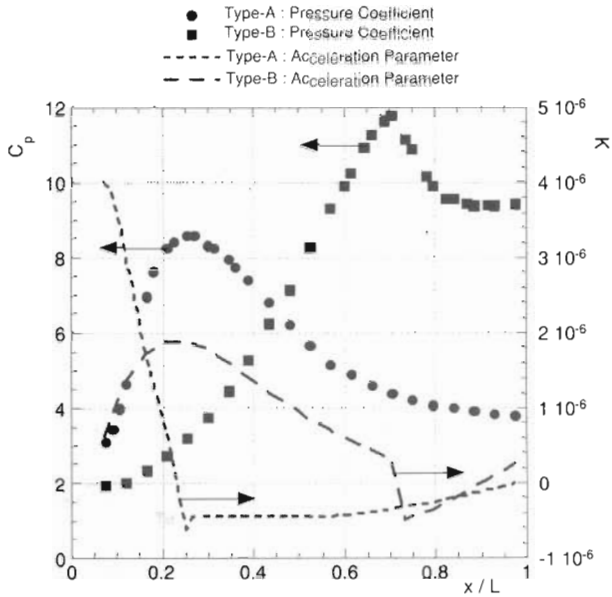

Fig. 5 Pressure coefficients and acceleration parameters for Type A and Type B

Note that the value, 3×10^{-6}, is considered to be a kind of threshold related to relaminarization of a turbulent boundary layer. Type B passage-contouring device produced gradual flow acceleration over about 3/4 surface of the test model and the averaged acceleration parameter was about 4×10^{-7}. The peak value of the acceleration became more than 1.5×10^{-6}.

Figure 6 shows ensemble-averaged velocity and turbulence intensity distributions of the incoming wakes for $d=5$ mm and $d=3$ mm, which were measured by the hot-wire probe located 200 mm upstream of the test model. These data were normalized with the inlet velocity. Maximum wake turbulence intensity reached about 8% for $d=5$ mm and about 5% for $d=3$ mm. The velocity deficit inside the wake was about 6% of the inlet velocity for $d=5$ mm and about 5% for $d=3$ mm. With the turbulence grid, the background turbulence intensity increased from 0.5% to 1.5%, while the peak values of velocity deficit and turbulence intensity did not exhibit substantial change even under the enhanced free-stream turbulence condition.

5. Results

5.1 Effects of wake passing upon transitional behavior

Type A contouring Fig. 7 shows instantaneous velocity signals measured for Test Case 1 and Test Case 2. These data, measured at $y/L=0.2\times10^{-3}$ for 14 locations, were normalized with the local velocity $U_e(x)$. Any interval between two adjacent velocity signals in these figures was proportional to the actual spatial interval between the corresponding measurement locations. Information on Re_2, Reynolds number based on the steady-state momentum thickness and the local velocity $U_e(x)$, was pro-

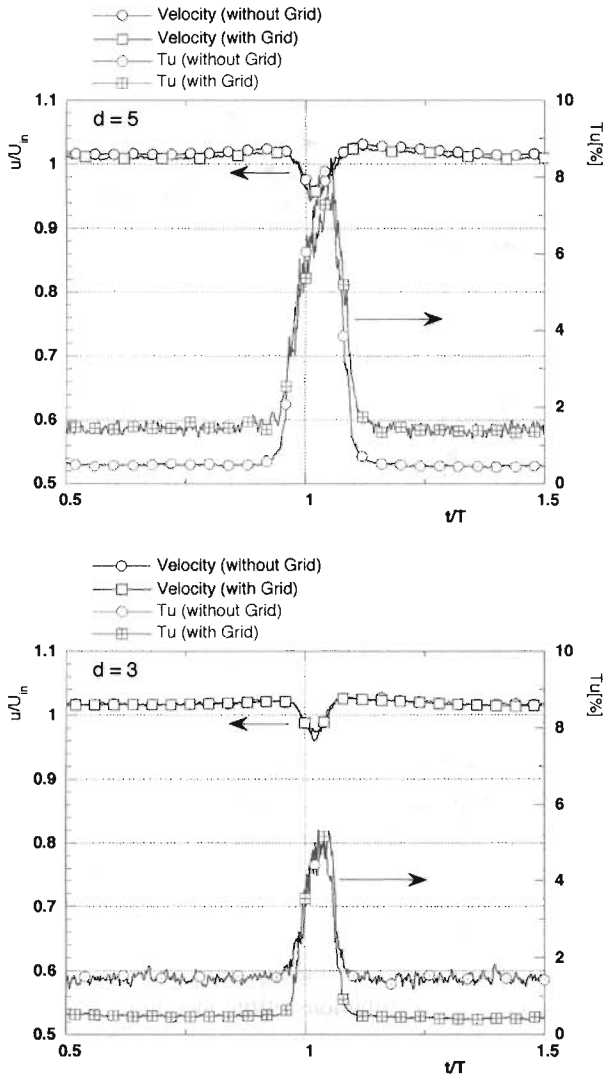

Fig. 6 Velocity and turbulent intensity distributions of the bar wake with and without turbulence grid (upper: d = 5 mm/lower: $d = 3$ mm)

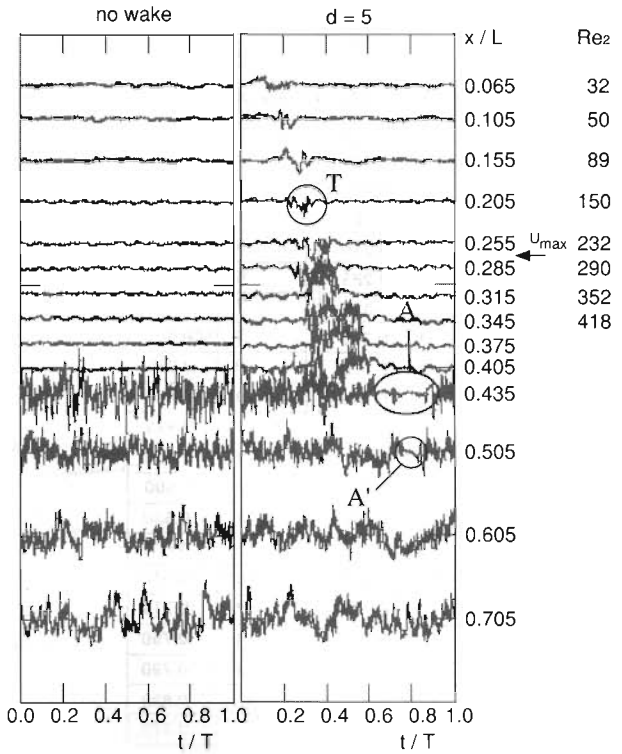

Fig. 7 Raw velocity signals for Test Case 1 (left) and Test Case 2 (right) measured at $y/L = 0.2 \times 10^{-3}$, showing wake-interaction with the boundary layer subjected to Type A pressure gradient

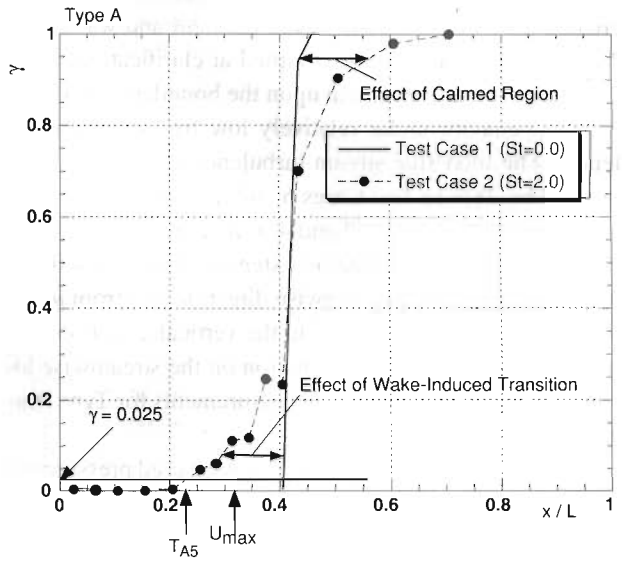

Fig. 8 Time-averaged intermittency for Test Case 1 and Test Case 2

vided to several velocity signals in this figure to seek for any relationship between wake-induced transition onset and the Reynolds number. In Test Case 1, the normalized velocity data abruptly exhibited intense fluctuation just after $x/L = 0.40$. This abrupt transition was also confirmed from the time-averaged intermittency factor shown in Fig. 8. In Test Case 2, the normalized velocity data contained clear traces of periodic wake passing over the test model whose envelopes tended to take a shape of wedge after the impact of the incoming wake upon the boundary layer. The appearance of this wedge-shaped envelopes of the traces implied that the wake passage eventually induced transition of the boundary layer through the production of turbulent spots. In fact, the wake-affected velocity signals began to be featured with intense fluctuation after $x/L = 0.205$, as indicated by the circle T. Note that the Reynolds number based on the momentum thickness at $x/L = 0.205$, was about 150. The position of the transition onset was also confirmed by the intermittency distribution in Fig. 8. The other feature to be mentioned as for the transitional behavior of the wake-affected boundary layer was the emergence of calmed region just after the wake passing, which is enclosed with the mark A in Fig. 7. The calmed region acted in such a way that the highly fluctuating boundary layer at $x/L = 0.435$ was calmed down to be

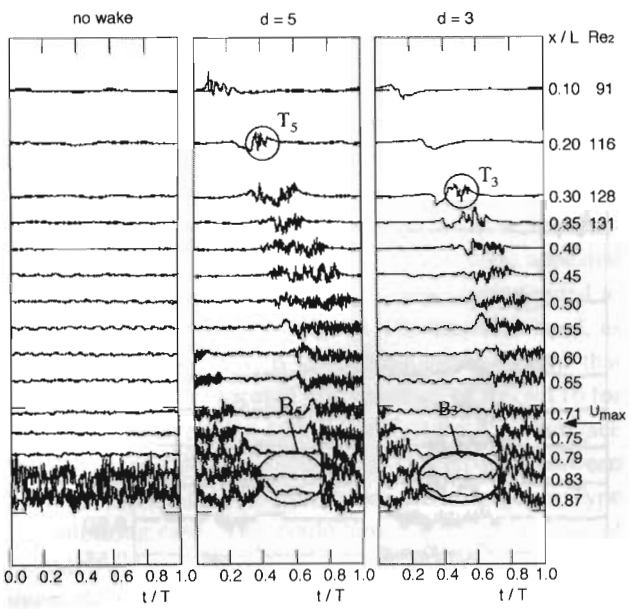

Fig. 9 Raw velocity signals for Test Case 3 (left) and Test Case 4 (right) measured at $y/L = 0.2 \times 10^{-3}$, showing wake-interaction with the boundary layer subjected to Type B pressure gradient

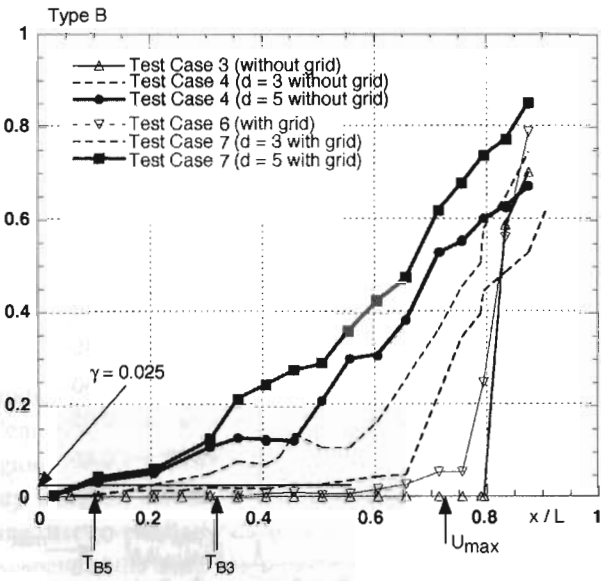

Fig. 10 Time-averaged intermittency for Type B contouring device

almost laminar. The effect of the calmed region remained at $x/L = 0.505$, which is marked with A. This rather long-lasting effect of the calmed region led to a relatively gradual transition process as shown in the intermittency factor of Fig. 8.

Type B contouring Fig. 9 illustrates instantaneous velocity signals for Test Case 3 and Test Case 4, the latter including the cases for $d = 5$ mm and $d = 3$ mm. Occurrence of the natural transition was delayed due to the long and gradual flow acceleration, where the transition took place between the measuring points #19 and #20 in Fig. 4. The velocity data for Test Case 4 with $d = 5$ mm revealed the appearance of wedge-shaped highly fluctuating velocity zones, which were generated by the wake passing and wake-induced turbulent spots. As shown by the circle T_5, wake-induced transition was likely to start around $x/L = 0.20$ where Re_2 was 116. The calmed region, designated B_5, then appeared just after the wake passage. As for the velocity data in Test Case 4 with $d = 3$ mm, the fluctuation inside the circle T_3 indicated that the wake-induced transition occurred a little later than that of the $d = 5$ mm case, which was due to the relatively weak turbulence intensity of the wake for $d = 3$ mm. The calmed region B_3 existed over the surface where the turbulent boundary layer would have been. This calmed region for $d = 3$ mm lasted longer than that for $d = 5$ mm because of the delayed transition in the $d = 3$ mm case.

Figure 10 demonstrates intermittency factors obtained in the cases using Type B contouring device. Note that not only the intermittency factors for the no-grid cases (Test Case 3 and Test Case 4) but also those for the cases with the grid (Test Case 6 and Test Case 7) are shown in this figure. A large difference was observed between the cases using the bars with $d = 5$ mm and $d = 3$ mm in the wake-induced transition process expressed by the development of the intermittency factor. The bar wakes for $d = 5$ mm eventually promoted the boundary layer transition in comparison with the case of $d = 3$ mm, which was probably due to the effect of the gradual acceleration, in other words, the modestly favorable pressure gradient responsible for preventing the boundary layer being affected by the relatively weak bar wakes of $d = 3$ mm from growing in the streamwise direction. After experiencing the maximum speed, the boundary layer subjected to the wakes of $d = 3$ mm bars rapidly advanced its pace of transition.

5.2 Effects of free-stream turbulence

Figure 11 depicts the wake-affected velocity signals acquired in Test Case 7 using the bars of $d = 5$ mm and $d = 3$ mm, where the inlet free-stream turbulence was elevated up to 1.5%. Interestingly, even under the flow acceleration, this modest elevation of the inlet free-stream turbulence appeared to have some impact on the transitional behavior of the boundary layer in terms of the intermittency factor as well as the emergence of some spikes in the signals. In fact, the intermittency factors shown in Fig. 10 demonstrates further promotion of the wake-induced transition under the influence of the enhanced turbulence intensity. Besides, spiky fluctuations, marked with C_5 and C_3, emerged between the two neighboring wake traces in the velocity signals after the location of the maximum speed. Much has remained unknown about the reason why these spikes occurred. One of the plausible reasonings for them was break down of streaks the enhanced free-stream

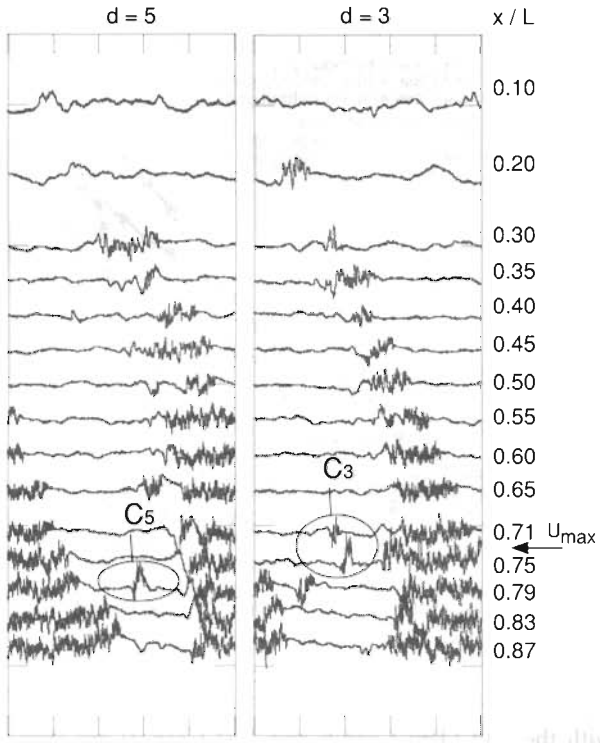

Fig. 11 Raw velocity signals for Test Case 7 using the bars with $d = 5$ mm (left) and $d = 3$ mm (right) measured at $y/L = 0.2 \times 10^{-3}$, showing the effects of enhanced free-stream turbulence upon wake-affected boundary layer transition

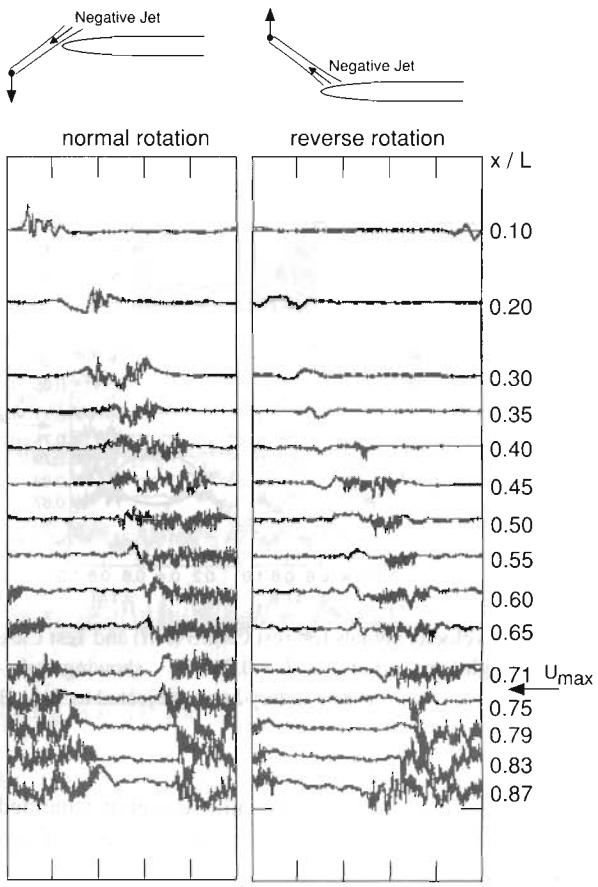

Fig. 12 Raw velocity signals for Test Case 4 (left: normal rotation) and Test Case 5 (right: reverse rotation) using the bars with $d = 5$ mm, which were measured at $y/L = 0.2 \times 10^{-3}$

turbulence left inside the boundary layer. As pointed out by Matsubara and Alfredson[9], streaks can be observed inside the boundary layer that is subjected to free-stream turbulence with more than 1% intensity, and are considered to be a major player in boundary layer bypass transition. In other words, the streak is responsible for the emergence of a turbulent spot via its instability process. Accordingly, in the present study, it was likely that streaks inside the boundary layer, which were generated by the free-stream turbulence and were in a stable condition due to the favorable pressure gradient, became unstable at or after the maximum velocity location, resulting in the emergence of the spikes, i.e., turbulent spots.

5.3 Effects of wake movement

Figure 12 clearly shows how the difference in the bar movement direction affected the transitional behavior of the boundary layer. In Test Case 5, where the wakes containing so-called negative jet effect were being convected over the boundary layer as shown above in the right column of this figure, the wake traces in the velocity data were not featured with any high-frequency fluctuations until $x/L = 0.350$. This was in contrast to the normal rotation case shown in the left column of Fig. 12. Similar findings were already reported by one of the present authors[10] as well as by Kittichaikarn et al.[11] In particular, Kittichaikarn et al. revealed from their flow-visualization using TLC that the wakes in the reverse rotation case eventually induced turbulent spots from a relatively narrow area on the surface compared to the case of the normal direction. Despite several experimental findings related to the effects of bar movement, less is known about the mechanism what actually causes the difference in the spot generation and the subsequent transition process of the boundary layer, and further studies are still needed.

6. Discussion on Transition Onset

Prediction of transition onset, especially in wake-induced bypass transition case, is a very challenging but important task that should be pursued in this study. There is a consensus among turbomachinery-related community that Mayle's correlation[1] as well as Abu-Ghannam, Show's correlation are well-established tools to predict the transition onset caused by free-stream turbulence. Mayle's correlation has a great benefit in actual applications because of its simple form consisting only of turbulence intensity (Tu), which is expressed as follows;

$$Re_{2tr} = 400 Tu^{-5/8}, \tag{12}$$

where Re_{2tr} is Reynolds number based on momentum

thickness at the onset point and Tu is in percentile. Interpreting maximum turbulence intensity attained in the wake as the free-stream turbulence in Eq. (12), at the same time using the turbulence intensities shown in Fig. 6, the transition onset can be expected to reside at $Re_{2tr} = 109$ for $d = 5$ mm and $Re_{2tr} = 146$ for $d = 3$ mm Taking advantage of the intermittency factor shown in Fig. 8, the transition for Type A contouring case with $d = 5$ mm appeared to start from around $Re_{2tr} = 150$, which corresponded to $x/L = 0.205$ (point T_{A5} in Fig. 8). On the other hand, as described before, Type B contouring cases showed that the transition onset located just upstream of $Re_2 = 116$ for $d = 5$ mm and at $Re_{2tr} = 122$ (point T_{B3}) for $d = 3$ mm (see Fig. 9 and the relevant discussion). Discrepancy between the experiments and the predictions seems larger in Type A contouring case. This could have happened because of the intense flow acceleration that weakened the turbulence intensity of the incoming wakes. It could be also mentioned that the stabilized boundary layer resisted the wake-induced transition longer than in the zero-pressure gradient case. Moreover, turbulent spot characteristics such as spread angle might have been affected by the favorable pressure gradient. Despite the fact that Mayle's correlation does not account for the factors described just in the above, it works fairly well even in the prediction of wake-induced boundary layer transition, provided that the maximum turbulence intensity of wake is used instead. Further relevant studies might be able to improve the correlation.

7. Discussion on Turbulent Spots Induced by Bar Wakes

Before drawing some conclusions from this study, it seems necessary to make some comment on turbulent spots induced by bar wakes. Most of the readers and most of the researchers working on bypass transition problems may imagine that when a bar wake impinges a flat plate, a number of turbulent spots, each of which takes an arrowhead shape growing in the streamwise direction under the influence of neighboring turbulent spots, appear inside the flat-plate boundary layer in alignment with each other along the bar wake direction. In a sense of ensemble-average, such clustered turbulent spots might be regarded as a two-dimensional and band-like highly turbulent zone. As described in this paper, the experimental findings surely support this recognition in terms of the propagation speed of the highly turbulent zones or the appearance of the calmed region, for example. Interestingly, however, very few studies have been made to reveal what is actually happening in the wake-affected boundary layer. Therefore, a question is now raised whether a turbulent spot induced by bar wake takes a shape of conventional arrowhead pointing downstream or not[13]. Much still remains unknown and relevant studies have just begun[14].

8. Conclusions

This study dealt with the detailed studies of boundary layer bypass transition caused by periodic bar-wake passage. Effects of the pressure gradients and the free-stream turbulence were examined in terms of temporal behaviors of the velocity signals as well as intermittency factors. The important findings in this study can be itemized as follows.

1) Wedge-shaped zones of high fluctuations were observed in the series of the measured raw velocity signals regardless of the types of passage-contouring device, indicating that the wake passage surely generated turbulent spots in the boundary layers. In addition, calmed regions clearly appeared just after the wake-induced velocity wedges. The intermittency factor in Type A contouring case revealed that the appearance of the calmed region suspended the completion of the wake-induced transition.

2) Comparing the experimental data with Mayle's correlation which was very popular and well established for zero-pressure gradient boundary layers, it was revealed that the favorable pressure gradients examined in this study delayed the transition onset, particularly in Type A contouring case with larger acceleration parameter.

3) The intermittency factors exhibited that moderately elevated inlet free-stream turbulence had a capability to promote the boundary layer transition under the flow-acceleration. Spiky velocity fluctuations were observed between two neighboring wake traces mainly after the flow started to decelerate. These spikes were probably due to break down of streaks induced by the free-stream turbulence, the break down which resulted in the emergence of turbulent spots.

4) Remarkable difference in the wake-induced transition was confirmed between in the normal and reverse rotation cases. This could be attributed to negative jet effects, although much remains to be examined in more detail to acquire the hidden mechanism causing the difference.

5) Mayle's correlation reasonably predicted wake-induced boundary layer transition onsets when the inlet maximum turbulence intensity of wake was used.

Acknowledgments

The authors are indebted to invaluable supports from Mr. F. Saito of Iwate University and the former student Mr. J. Takahashi.

References

(1) Mayle, R.E., The Role of Laminar-Turbulent Transition in Gas Turbine Engines, ASME Journal of Turbomachinery, Vol.113 (1991), pp.509–537.

(2) Walker, G.J., The Role of Laminar-Turbulent Transition in Gas Turbine Engines: A Discussion, ASME Journal Turbomachinery, Vol.115 (1993), pp.207–217.

(3) Solomon, W.J., Unsteady Boundary Layer Transition

Axial Compressor Blades, Ph.D. Thesis, University of Tasmania, (1996).
(4) Funazaki, K., Unsteady Boundary Layers on a Flat Plate Disturbed by Periodic Wakes: Part I—Measurement of Wake-Affected Heat Transfer and Wake Induced Transition Model, ASME Journal of Turbomachinery, Vol.118 (1996), pp.327–336.
(5) Funazaki, K., Unsteady Boundary Layers on a Flat Plate Disturbed by Periodic Wakes: Part II—Measurements of Unsteady Boundary Layers and Discussion, ASME Journal of Turbomachinery, Vol.118 (1996), pp.337–346.
(6) Halstead, D.E., Wisler, D.C., Okiishi, T.H., Walker, G.J., Hodson, H.P. and Shin, H.W., Boundary Layer Development in Axial Compressors and Turbines: Part1 of 4—Composite Picture, ASME Journal of Turbomachinery, Vol.119 (1997), pp.114–127.
(7) Ottavy, X., Vilmin, S., Opoka, M. and Hodson, H., The Effects of Wake-Passing Unsteadiness over a Highly-Loaded Compressor-Like Flat Plate, ASME Paper GT-2002-30354, (2002).
(8) Kline, S.J. and McClintock, F.A., Describing Uncertainties in Single-Sample Experiments, Mechanical Engineering, Vol.75, Jan. (1953), pp.3–8.
(9) Matsubara, M. and Alfredson, P.H., Disturbance Growth in Boundary Layers Subjected to Free-Stream Turbulence, Journal of Fluid Mechanics, Vol.430 (2001), pp.149–168.
(10) Funazaki, K., Kitazawa, T., Koizumi, K. and Tanuma, T., Studies on Wake-Disturbed Boundary Layers under the Influences of Favorable Pressure Gradient and Free-Stream Turbulence-PartI: Experimental Setup and Discussions on Transition Model, ASME Paper 97-GT-52, (1997).
(11) Kittichaikarn, C., Ireland, P.T., Zhong, S. and Hodson, H.P., An Investigation on the Onset of Wake-Induced Transition and Turbulent Spot Production Rate Using Thermochromic Liquid Crystals, ASME Paper 99-GT-126, (1999).
(12) Abu-Ghannam, B.J. and Shaw, R., Natural Transition of Boundary Layers: The Effects of Turbulence, Pressure Gradient, and Flow History, Journal of Mechanical Engineering Science, Vol.22, No.5 (1980), pp.213–228.
(13) Wu, X., Jacobs, R.G., Hunt, J.C.R. and Durbin, P.A., Simulation of Boundary Layer Transition Induced by Periodically Passing Wakes, Journal of Fluid Mechanics, Vol.398 (1999), pp.109–153.
(14) Funazaki, K., Wakita, Y. and Otsuki, T., Studies on Bypass Transition of a Boundary Layer Subjected to Localized Periodic External Disturbances, ASME Paper, GT2004-53305, (2004).
(15) Falco, R.E. and Gendrich, C.P., The Turbulent Burst Detection Algorithm of Z. Zaric, Edited by Kline, S.J. and Afgan, N.H., Near-Wall Turbulence 1988 Z. Zaric Memorial Conference, (1990), pp.911–931, Hemisphere.
(16) Kaszata, R.W., Experimental Investigation of Transition to Turbulence as Affected by Passing Wakes, Ph. D. Thesis, University of Minnesota, (2000).